

# Methyl- $\beta$ -cyclodextrin Inclusion Complex with $\beta$ -Caryophyllene: Preparation, Characterization, and Improvement of Pharmacological Activities

Pauline S. Santos,<sup>†</sup> Luan K. M. Souza,<sup>‡</sup> Thiago S. L. Araújo,<sup>‡</sup> Jand Venes R. Medeiros,<sup>‡</sup> Sandra C. C. Nunes,<sup>§</sup> Rui A. Carvalho,<sup>||</sup> Alberto C. C. Pais,<sup>§</sup> Francisco J. B. Veiga,<sup>⊥</sup> Lívio C. C. Nunes,<sup>†</sup> and Ana Figueiras<sup>\*,⊥,||</sup>

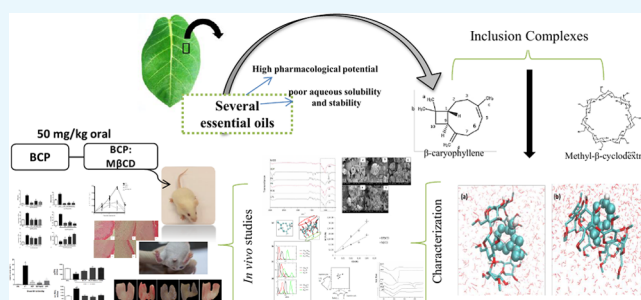
<sup>†</sup>Postgraduate Program of Northeast Biotechnology Network, Faculty of Pharmacy, Federal University of Piauí, Teresina, 64049-550, Piauí, Brazil

<sup>‡</sup>Northeast Biotechnology Network, Postgraduate Program in Biotechnology, Federal University of Piauí, 64202-020, Parnaíba, Piauí, Brazil

<sup>§</sup>Department of Chemistry, CQC, <sup>||</sup>Department of Biochemistry, NMR Spectroscopy Center, Faculty of Sciences and Technology, and <sup>⊥</sup>REQUIMTE/LAQV, Group of Pharmaceutical Technology, Faculty of Pharmacy, University of Coimbra, 3000-548 Coimbra, Portugal

## Supporting Information

**ABSTRACT:**  $\beta$ -Caryophyllene (BCP) is a sesquiterpene that shows high potential in pharmacological applications. However, these have been drastically limited by the respective volatility and poor water solubility. The present study investigates the formation of inclusion complexes between BCP and methyl- $\beta$ -cyclodextrin (M $\beta$ CD) and shows that these complexes promote a significant improvement of the anti-inflammatory, gastric protection, and antioxidant activities relative to neat BCP. It is shown that the solubility of BCP is significantly increased through complexation in phase solubility studies. Inclusion complexes with M $\beta$ CD in solid state were prepared by three different methods, kneading, rotary evaporation, and lyophilization, with the latter confirmed by differential scanning calorimetry, Fourier transformed infrared spectroscopy, scanning electron microscopy, <sup>1</sup>H NMR spectroscopy, and molecular dynamics studies. This study provides for the first time a full characterization of inclusion complexes between BCP and M $\beta$ CD and highlights the impact of complex formation upon pharmacological activity.



## INTRODUCTION

$\beta$ -Caryophyllene (BCP) (Figure 1B) is one of the main components of the essential oil obtained from a large number of species of plants and spices used for medicinal purposes, for example, Korean mint (*Agastache rugosa*<sup>1</sup>), copaiba oil (*Copaifera langsdorffii*<sup>2</sup>), and clove (*Syzygium aromaticum*<sup>3</sup>). This sesquiterpene was approved by the Food and Drug Administration (21 CFR 121.1164) as a food additive, and it was recommended to be used as functional food and dietary supplement due to its antioxidant properties.<sup>4,5</sup>

Over time, this compound has attracted considerable attention of chemists and pharmacologists because of its variety of biological activities as painkiller,<sup>6</sup> anticancer,<sup>7</sup> antioxidant, antimicrobial,<sup>8</sup> anxiolytic, antidepressive,<sup>9</sup> renal protector,<sup>10</sup> hepatic protector,<sup>1</sup> and neural protector.<sup>11</sup> BCP has also been reported to exert strong anti-inflammatory effects in numerous studies for more than a decade.<sup>12–16</sup> It is worth mentioning that BCP promotes this anti-inflammatory action without causing

gastric mucosal injury and that it might be beneficial to treat gastrointestinal disorders.<sup>12,17,18</sup>

Despite this recognized pharmacological potential, the dissolution of BCP from oral preparations has been shown to be low due to its poor water solubility and this characteristic is considered a challenge for the formulation of effective oral dosage forms. Beyond the low solubility, BCP shows characteristics such as volatility, strong smell, described as spicy or ligneous, and easy oxidation when exposed to light and oxygen.<sup>19,20</sup> Some strategies have been assessed to overcome these limitations. Among them, the complexation with cyclodextrins (CDs) shows a large application in the pharmaceutical industry because CDs can both improve drug solubility and stability by complexation.<sup>21–23</sup> Moreover, they

Received: September 27, 2017

Accepted: November 27, 2017

Published: December 18, 2017

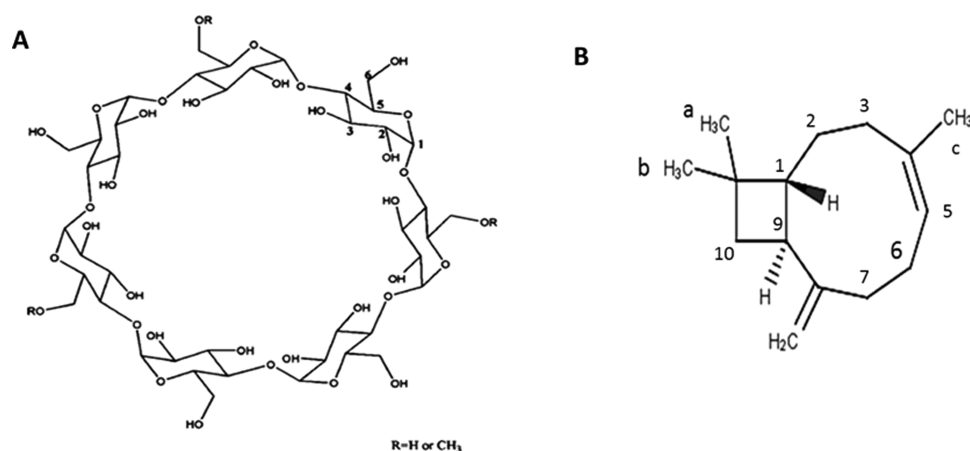


**Figure 1.** Molecular structures of methyl- $\beta$ -cyclodextrin (A) and  $\beta$ -caryophyllene (B).

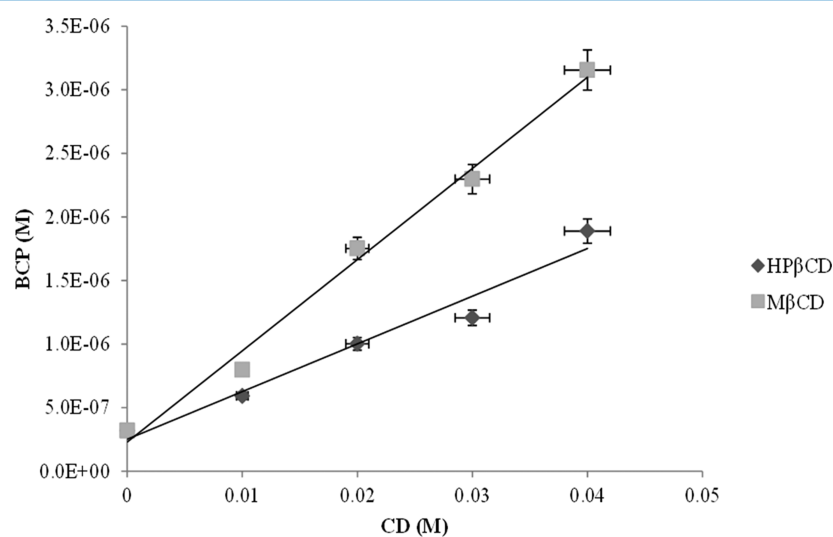


**Figure 2.** Phase solubility studies of BCP with M $\beta$ CD and 2-hydroxypropyl- $\beta$ -cyclodextrin (HP $\beta$ CD) in aqueous solution at  $25 \pm 2$  °C. The values are mean  $\pm$  % standard deviation.

can promote the controlled release of some insoluble terpenes, such as linalool,<sup>24</sup> limonene,<sup>25</sup> terpineol,<sup>26</sup> and citronella.<sup>27</sup>

The complexation of BCP with  $\beta$ CD was previously demonstrated and claimed to be a viable alternative to improve the oral bioavailability of this compound when administrated in rats.<sup>28</sup> Besides, the BCP<sup>16</sup> and the essential oil of *Hyptis pectinate*,<sup>29</sup> which contains 54.07% of BCP also developed in inclusion complexes (ICs) with  $\beta$ CD, showed enhanced analgesic pharmacological effects in mice. Nevertheless, the formation of inclusion complexes of BCP with methyl- $\beta$ -cyclodextrin (M $\beta$ CD) has not been addressed.

In this research, we aim to investigate the preparation and characterization of inclusion complex formed by BCP and M $\beta$ CD. Our main interest is to explore this inclusion complex as an anti-inflammatory and gastric protection oral formulation. For this purpose, phase solubility studies were performed. Subsequently, complexes in solid state were prepared by kneading (KN), rotary evaporation (ROE), and lyophilization (Lph). The obtained binary systems were characterized using several techniques, namely, differential scanning calorimetry (DSC), Fourier transformed infrared spectroscopy (FTIR), scanning electron microscopy (SEM), nuclear magnetic resonance spectroscopy (<sup>1</sup>H NMR), rotating-frame nuclear Overhauser effect (ROESY) spectroscopy, and molecular

dynamics (MD) simulation. In addition, anti-inflammatory, antioxidant, and gastric protective studies were conducted in mice to assess the potential of inclusion complex to improve the activities relative to neat BCP orally.

## RESULTS AND DISCUSSION

**Phase Solubility Studies.** A calibration curve of BCP was constructed at 203 nm using a hydroalcoholic solution (1:9, v/v) as solvent ( $R^2 = 0.997$ ).<sup>28,30</sup> Phase solubility studies (Figure 2) showed that BCP solubility increases linearly with CD concentration and the slope is smaller than unity, over the entire concentration range studied, indicating an  $A_L$ -type diagram with the formation of inclusion complexes with 1:1 stoichiometry for both cyclodextrins.<sup>31</sup>

The determination of the stability constant of the inclusion complexes is a crucial point for the evaluation of their effectiveness because the different possible effects related to the complex formation all rely on the stability of the complexes formed.<sup>32,33</sup> Low values of  $K_s$  indicate a weak interaction and a higher amount of free ligand, whereas higher values of  $K_s$  indicate that the equilibrium is shifted toward the formation of the complex. Values within the 100–1000  $M^{-1}$  range are considered ideal.<sup>34–36</sup>

**Table 1.** Parameters Obtained from the Phase Solubility Diagrams of the Systems BCP/*M*βCD and BCP/HPβCD<sup>a</sup>

	diagram type	slope	$S_0$ ( $M \times 10^{-7}$ )	$S_f$ ( $M \times 10^{-7}$ )	$K_s$ ( $M^{-1}$ )
BCP/HPβCD	$A_L$	$4 \times 10^{-5}$	3.20	18.88	125.00
BCP/ <i>M</i> βCD	$A_L$	$7 \times 10^{-5}$	3.20	31.54	218.76

<sup>a</sup> $S_0$ , BCP intrinsic solubility;  $S_f$ , BCP concentration in the presence of the maximum concentration of CD;  $K_s$ , apparent stability constants.

Table 1 shows the  $K_s$  values calculated for the inclusion complexes prepared with both cyclodextrins. This value was higher for the complexation with *M*βCD (218.76  $M^{-1}$ ) compared to HPβCD (125.00  $M^{-1}$ ), indicating a stronger interaction between BCP and *M*βCD in aqueous solution. The BCP solubility increased, approximately, 7- and 10-fold in the presence of the maximum concentrations of HPβCD and *M*βCD (40 mM), respectively, compared to  $S_0$ . Recently, Rakmai et al.<sup>30</sup> have demonstrated  $K_s$  values of 104.5 and 132.8  $M^{-1}$  at 25 and 35 °C, respectively, for the inclusion complex between BCP and HPβCD, corroborating with the demonstrated results. However, there are still no data regarding BCP inclusion complexes with *M*βCD that in our study demonstrated to promote a greater solubilization for this sesquiterpene in the phase solubility study. Considering the results obtained in aqueous solution, *M*βCD was selected to prepare and characterize inclusion complexes with BCP in the solid state.

**<sup>1</sup>H NMR Spectroscopy.** <sup>1</sup>H NMR spectroscopy analysis was performed to elucidate the structure of BCP/*M*βCD inclusion complexes. In the presence of the BCP, notable upfield shifts for H3 and H5 were observed (see Table 2) in the

**Table 2.** Chemical Shifts Corresponding to *M*βCD in Free and Complexed States

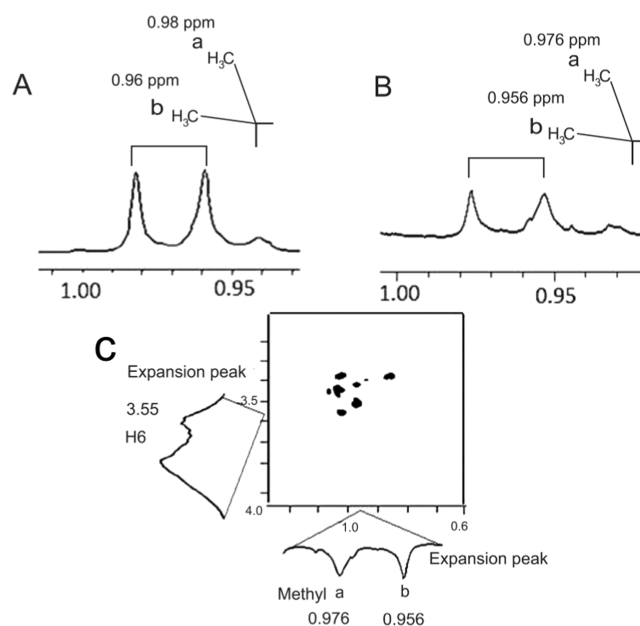
assignments	<i>M</i> βCD, $\delta$ (ppm)	BCP/ <i>M</i> βCD, $\delta$ (ppm)	$\Delta\delta$ (ppm)
H3	3.743	3.501	-0.242
H5	3.609	3.493	-0.116
H6	3.558	3.482	-0.076
methyl-6'	3.323	3.241	-0.082

*M*βCD spectrum, which demonstrated a clear involvement of these protons in host–guest interactions. The order of the upfield shifts was found to be H3 ( $\Delta\delta = -0.242$  ppm) > H5 ( $\Delta\delta = -0.116$  ppm). Both protons are located inside the CD cavity, and H3 protons are near the wide side of the cyclodextrin. These upfield shifts suggest that the entrance of the drug in the cavity occurs preferentially by the wide side. However, pronounced upfield shifts were also observed for H6 and methyl-6', which are located near H5 protons, in the narrow side of the cavity, suggesting that the establishment of drug–cyclodextrin interactions can also occur by the narrow side.

The  $\delta$  and corresponding  $\Delta\delta$  values for selected BCP protons were followed to observe their implication in the establishment of interactions with *M*βCD (Table 3). Figure 3 reports expansions of the <sup>1</sup>H NMR spectra of those regions in the absence (A) and presence (B) of *M*βCD. The observed

**Table 3.** Chemical Shifts Corresponding to BCP in Free and Complexed States

assignments	BCP, $\delta$ (ppm)	BCP/ <i>M</i> βCD, $\delta$ (ppm)	$\Delta\delta$ (ppm)
methyl a	0.98	0.976	-0.004
methyl b	0.96	0.956	-0.004

**Figure 3.** Expansion of the <sup>1</sup>H NMR spectra of BCP in the free state (A) and complexed with *M*βCD (B). ROESY expansion in the region of the interaction between BCP and *M*βCD (C).

upfield shifts indicate that methyl “a” and methyl “b” are involved in the complexation with the CD, confirming the hypothesis that this part of the BCP molecule is inside the CD cavity, but the magnitude of the values is compatible with a weak interaction.

**ROESY Spectroscopy.** Expansions of the ROESY spectra of BCP/*M*βCD inclusion complexes are reported in Figure 3C. These bidimensional experiments show intermolecular cross-peaks between H6 protons of *M*βCD and methyl protons of BCP, namely, methyl a and methyl b. These observations are consistent with the occurrence of interactions between BCP methyl groups (a and b) and H6 protons of the CD, confirming the partial inclusion of the drug in cyclodextrin cavity by the narrow side or complete inclusion by the wide side. The computer simulation indicates the possibility of this last hypothesis (see Figure 4B, panel b), showing an almost complete inclusion of the molecule by the wide side as demonstrated when inspected the orientation of the BCP in the complex by the part of the molecule that contain the carbon 10, which is close to the methyl groups a and b.

**Molecular Dynamics Simulations.** To obtain further molecular detail on the complexation between *M*βCD and BCP in solution, the distance between selected points in the *M*βCD and the drug molecule was monitored. The results depicted in Figure 4A show the inclusion of the drug molecule in the CD ring and its relative position inside the *M*βCD cavity. Panel (a) represents the distance between the center of mass of the two molecules and the distance between each portal of the *M*βCD and the center of mass of the drug. The curves show that the inclusion of the drug occurs and that it is preferentially located

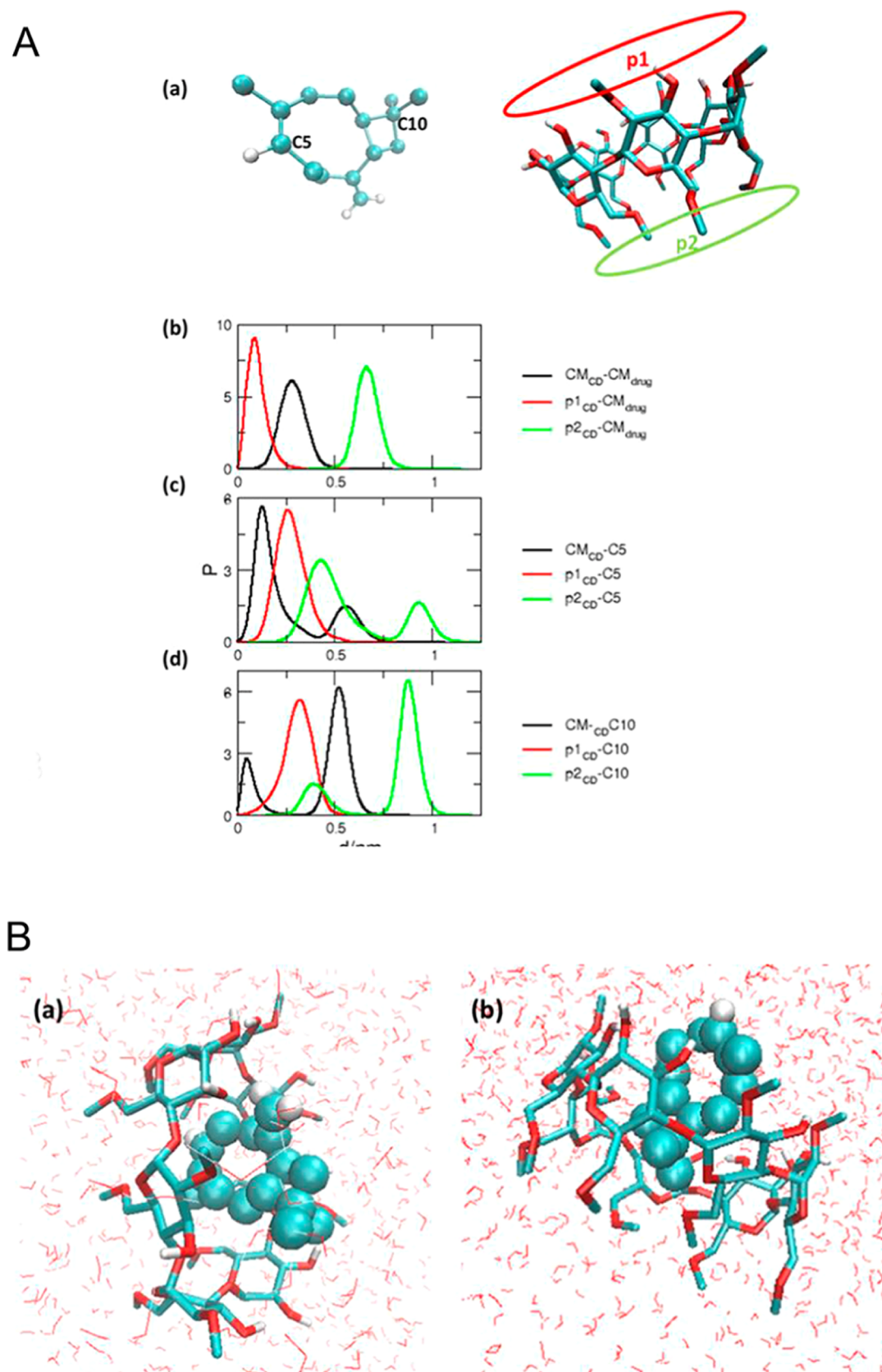


**Figure 4.** (A) Distribution of distances from  $M\beta\text{CD}$  to BCP: (a) points in the BCP molecule considered to evaluate inclusion together with the notation attributed to each portal of the  $M\beta\text{CD}$  ( $\text{p1}$  for the portal with the OH substituents and  $\text{p2}$  for the  $\text{CH}_2\text{OCH}_3$ -substituted portal); (b) distance from the center of mass (CM) and from  $\text{p1}$  and  $\text{p2}$  to the CM of the BCP; (c) distribution of distances between CM,  $\text{p1}$  and  $\text{p2}$  of  $M\beta\text{CD}$ , and the  $\text{C5}$  atom of the BCP; (d) distances from CM,  $\text{p1}$  and  $\text{p2}$  of  $M\beta\text{CD}$  to  $\text{C10}$  atom of the BCP molecule. (B) Snapshots extracted from the 60 ns of the production run at 298 K representing some characteristic configurations found for the system BCP/ $M\beta\text{CD}$ .

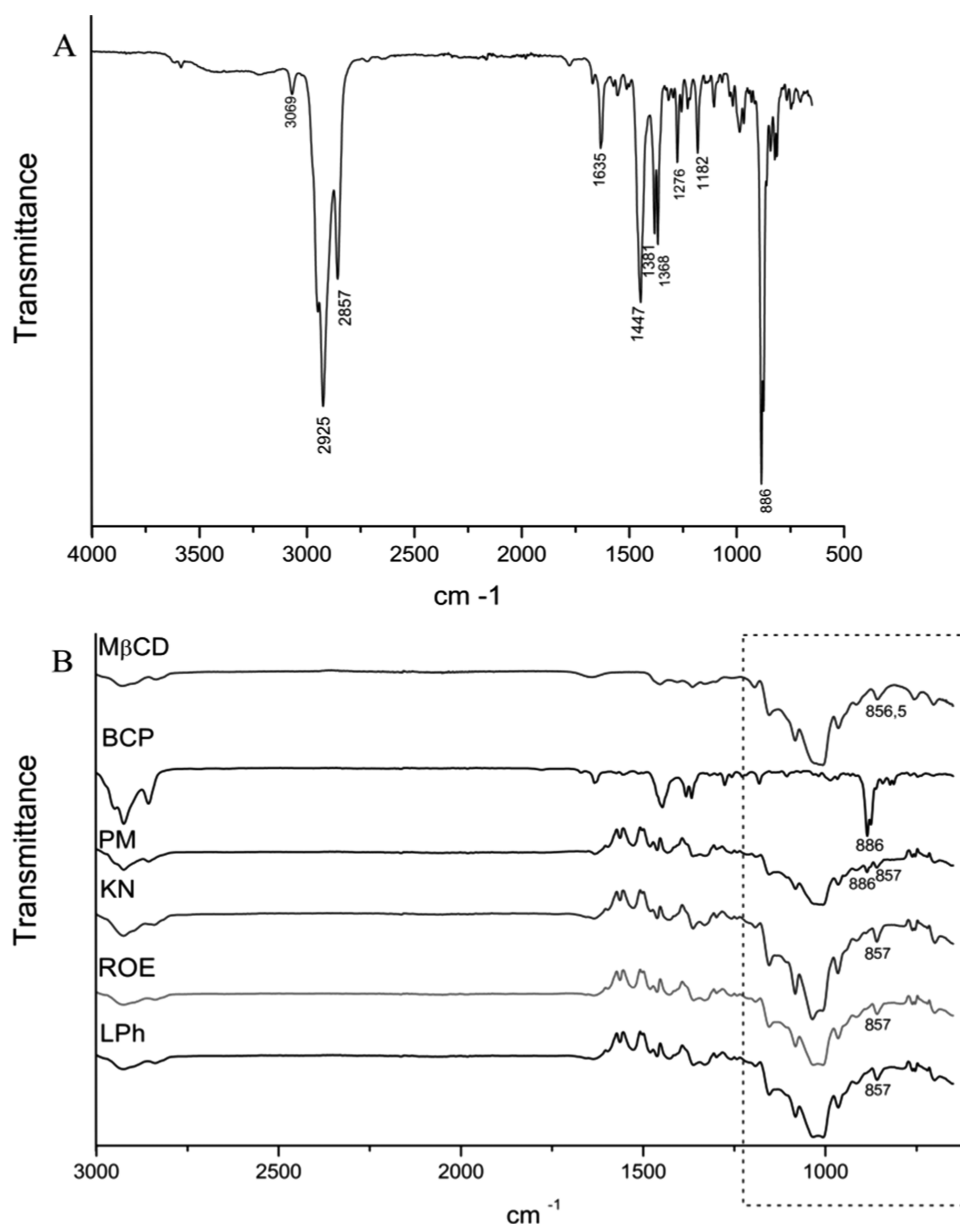


**Figure 5.** (A) FTIR spectrum of BCP. (B) FTIR spectra of  $M\beta$ CD, BCP, physical mixture (PM), and inclusion complexes obtained by KN, ROE, and LPh methods.

near to portal 1, which is the wide side. This is in fact in accordance with the snapshots presented in Figure 4B. This hypothesis has been demonstrated in  $^1\text{H}$  NMR when upfield shifts for H3 and H5 of  $M\beta$ CD were observed.

Additionally, to inspect the orientation of the BCP molecule in the complex, the distance between two opposite points in the drug and the center of mass of  $M\beta$ CD and each of its portals was also inspected. The curves presented in panels (b) and (c) of Figure 4A show that inclusion occurs preferentially by the C5 region of BCP (see Figure 4B, panel a), although the inclusion can also occur by the C10 part of the molecule (Figure 4B, panel b). The results also show an almost complete inclusion of the molecule. Thus, molecular dynamics suggest the possibility of existence of a new conformation (panel a) for the complex, in addition to that evidenced by NMR studies (panel b).

**Fourier Transform Infrared (FTIR) Spectroscopy.** The FTIR spectra of  $M\beta$ CD, BCP, physical mixture (PM), and

binary systems are represented in Figure 5. The infrared spectrum of BCP (Figure 5A) showed absorption bands of stretching vibrations at 3069 and 1447  $\text{cm}^{-1}$  of  $=\text{CH}$ . At 1635  $\text{cm}^{-1}$  appears a stretching vibration related to  $\text{C}=\text{C}$  bond. The double band at 1381 and 1368  $\text{cm}^{-1}$  of symmetrical deformation of  $-\text{CH}_3$  can be ascribed to two methyl groups connected to the same carbon atom. Methylenic hydrogens originate two CH stretching bands observed at 2925  $\text{cm}^{-1}$  (asymmetric stretching) and 2857  $\text{cm}^{-1}$  (symmetric stretching) that are characteristic of  $\text{CH}_2$  groups. The most intense band for BCP was observed at 886  $\text{cm}^{-1}$  assigned to out-of-plane deformation vibration of  $=\text{CH}$  characterizing the molecule.<sup>8,16,28,37</sup>

The FTIR spectrum of  $M\beta$ CD (Figure 5B) shows a large band at 3385  $\text{cm}^{-1}$  (O–H stretching), 2928  $\text{cm}^{-1}$  (stretching C–H), and 1193, 1082, and 1022  $\text{cm}^{-1}$  (C–O– stretching compatible to the bonds on ether and hydroxyl groups). The spectrum of the PM presents the characteristic absorption band

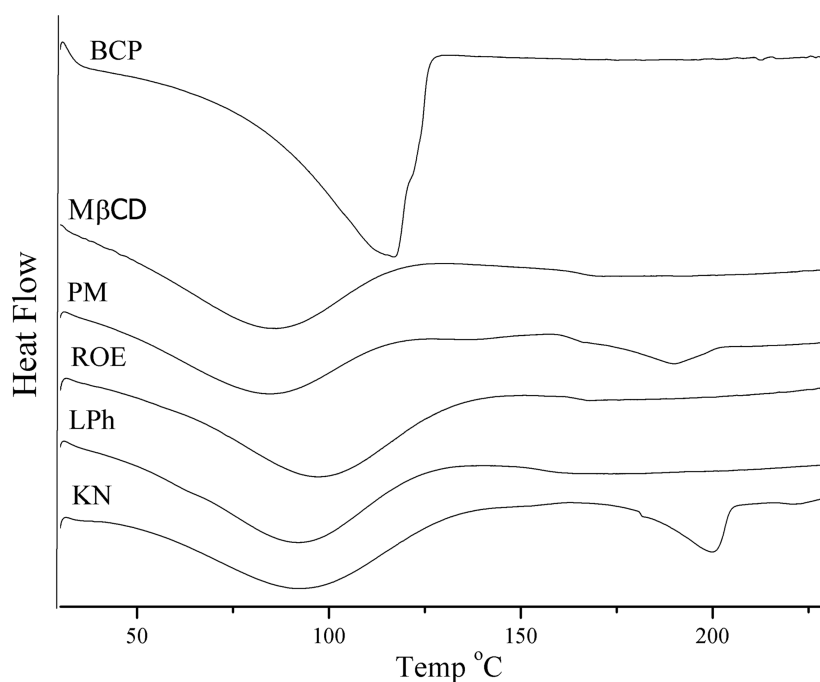


**Figure 6.** DSC thermograms of BCP,  $M\beta$ CD physical mixture (PM), and the inclusion complexes obtained by ROE, LPh, and KN.

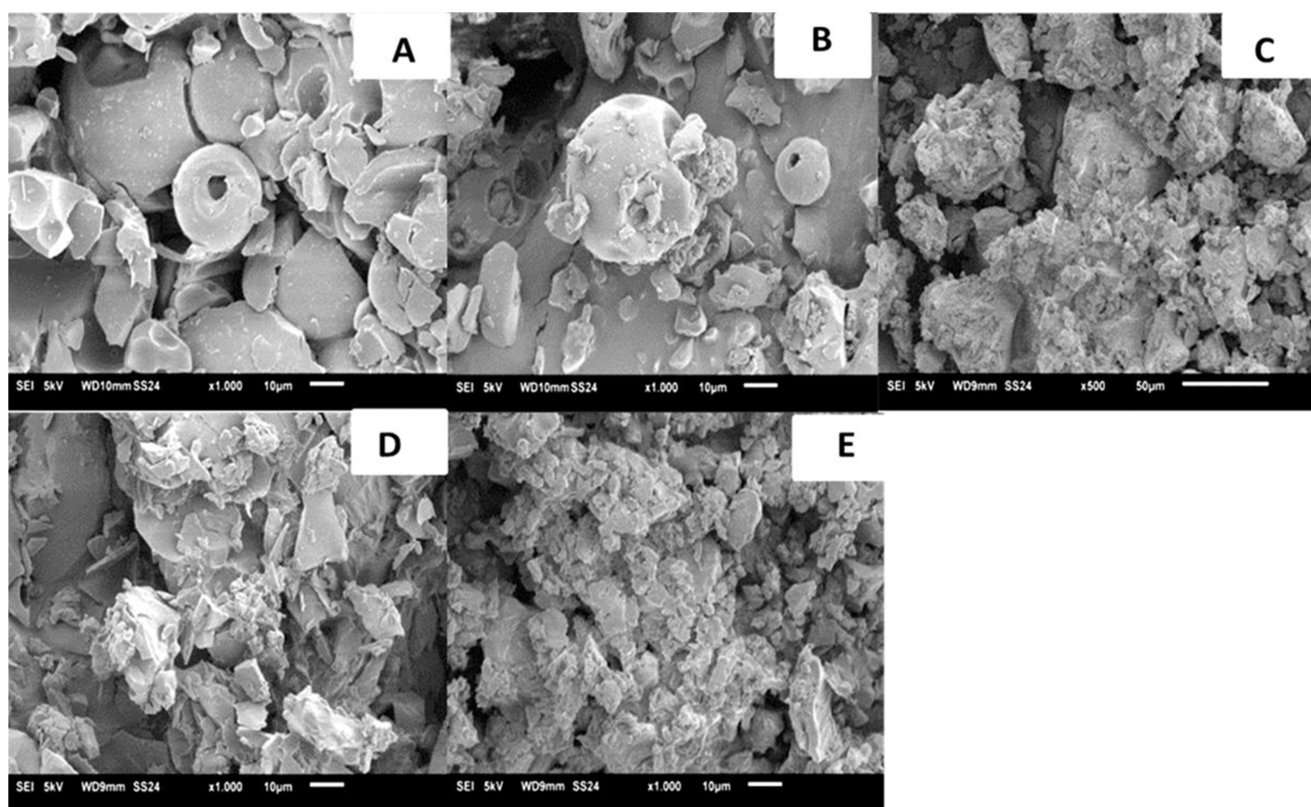


**Figure 7.** Scanning electron microphotographs of  $M\beta$ CD (A), PM (B), and the complexes prepared by KN (C), ROE (D), and LPh (E) methods at a magnification factor of 1000 $\times$ .

of BCP at  $886\text{ cm}^{-1}$  (as emphasized in Figure 5B) although its intensity is weaker. However, this band is not observed when the spectra of the complexes were analyzed, probably due to a restriction of the vibration related to the complexation process. This corroborates the results already obtained for the complexes obtained between BCP and  $\beta$ CD.<sup>28</sup> In the spectrum

of the inclusion complexes, few features were observed to be identical to BCP. Those changes can be ascribed to the formation of the inclusion complex related to the intermolecular bonds between BCP and  $M\beta$ CD.

**Differential Scanning Calorimetry (DSC).** The DSC technique proved to be a very powerful analytic tool to

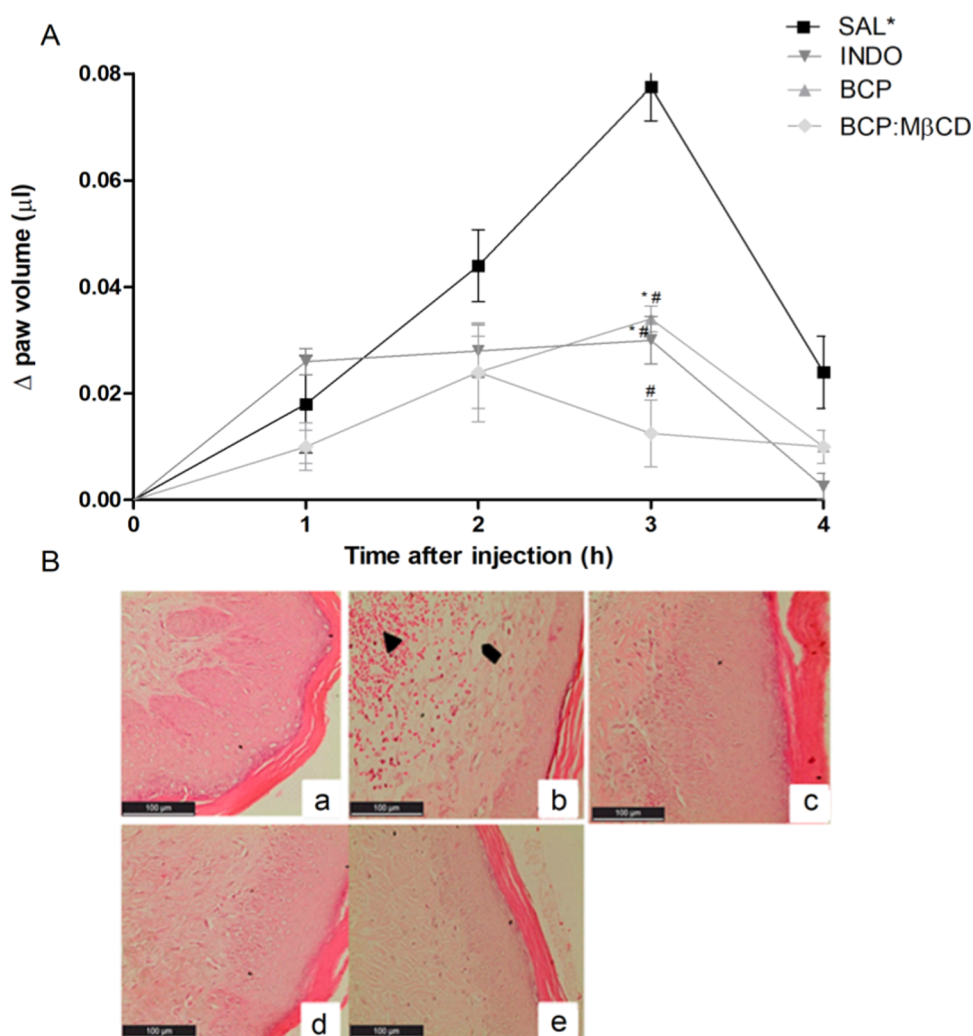


**Figure 8.** (A) Effects of BCP and BCP/M $\beta$ CD on edema paw inflammation induced by carrageenan. Animals were pretreated with BCP, BCP/M $\beta$ CD 50 mg/kg orally, or indomethacin (INDO, 10 mg/kg, intraperitoneally (ip)) # $p$  < 0.05 compared to Sal\*; \* $p$  < 0.05 compared to BCP/M $\beta$ CD. (B) Histological examination of paw tissue sections 3 h after carrageenan injection: (a) vehicle control (Sal), (b) carrageenan control (Sal\*), (c) treated with BCP, (d) treated with BCP/M $\beta$ CD, and (e) treated with standard drug indomethacin.

characterize the interactions among drugs and CDs in the solid state. When guest molecules are stabilized in CD cavities, their melting, boiling, or sublimation peaks are generally shifted to a different temperature or disappear.<sup>38–40</sup> The thermal behaviors of the pure components and binary systems are represented in Figure 6.

The thermogram of M $\beta$ CD reveals an endothermic event between 43 and 120 °C, which corresponds to the loss of water molecules.<sup>41</sup> BCP revealed one endothermic event between 45 and 127 °C ( $T_{\text{peak}}$  116 °C) assigned to its volatilization.<sup>16</sup> On the thermogram of the PM, the endothermic M $\beta$ CD loss of water event remained unchanged and an additional endothermic event between 160 and 200 °C ( $T_{\text{peak}}$  = 190 °C) was observed, which can be ascribed to the presence of BCP. The residual presence of the volatilization peak of the BCP in physical mixtures, although displaced, is indicative of the existence of free BCP molecules.<sup>22,29,42</sup>

Concerning the thermal curves of the binary systems (ROE, LPh, and KN), the dehydration signals of M $\beta$ CD were observed to be smaller and displaced, indicating a possible change of the activation energy necessary to the dehydration of

M $\beta$ CD due to the establishment of interactions in solid state with BCP.<sup>42,43</sup>

In the system obtained by the KN, the endothermic peak characteristic of the drug is displaced to a higher temperature (200 °C), suggesting a partial complexation between BCP and M $\beta$ CD. However, in the thermograms of the complexes prepared by ROE and LPh methods, the BCP volatilization peak was not observed. The absence of this peak indicates the formation of inclusion complexes in solid state and a more stable interaction between the drug and the M $\beta$ CD in these systems.<sup>44–46</sup>

**Scanning Electron Microscopy (SEM).** Scanning electron microscopy (SEM) is a qualitative method that allows the study of the structural aspect of the raw material and the products obtained by complexation with cyclodextrins. Figure 7 shows the microphotographs of M $\beta$ CD (A) constituted by spherical particles, which can be also observed in the PM (B). However, in the microphotographs of the complexes obtained by the KN (C), ROE (D), and LPh (E) methods, it is possible to observe the presence of irregular amorphous particles, in which the original morphology of M $\beta$ CD disappeared. Those changes on the surface structure of the isolated compounds indicate the

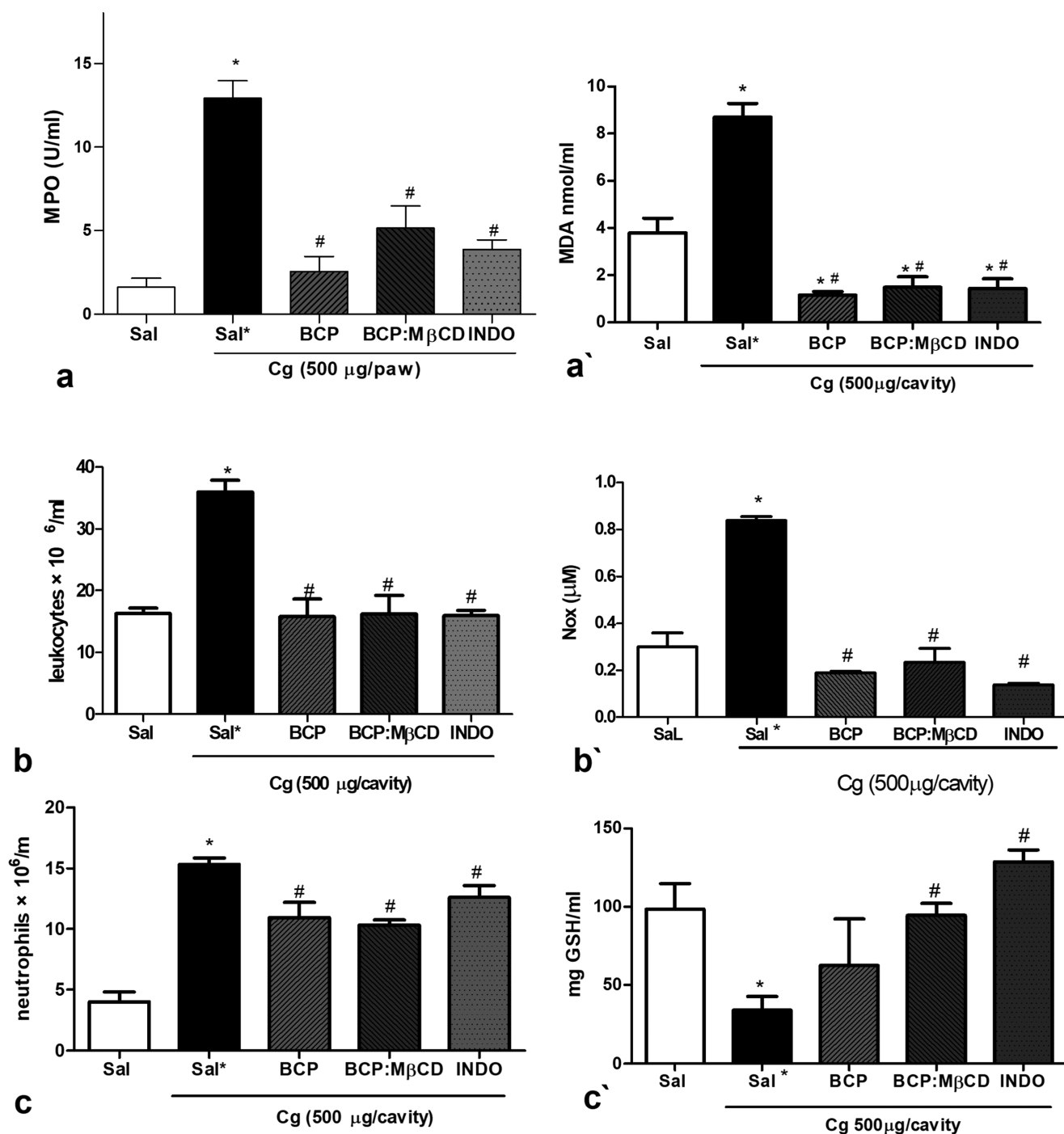


**Figure 9.** Anti-inflammatory and antioxidant effects of BCP and BCP/M $\beta$ CD. Myeloperoxidase (MPO): (a) activity was detected in the paw tissue after 4 h; (b, c) total counts of leukocytes and neutrophils, respectively, per cavity on carrageenan-induced peritonitis in mice. (a') Malondialdehyde (MDA), (b') glutathione (GSH), and (c') nitrite levels in the peritoneal exudate 4 h after carrageenan administration. Values are expressed as mean  $\pm$  SEM; \* $p$  < 0.05 compared to the Sal group; # $p$  < 0.05 compared to the carrageenan group (Sal\*). Statistical analysis was performed using analysis of variance followed by the Newman–Keuls test.

establishment of interactions with a new phase formation.<sup>29,41,47,48</sup>

Therefore, it is possible to conclude that drastic changes in the particles' form and aspect were introduced, corroborating the other results. Studies have demonstrated that the LPh technique substantially improves the dissolution characteristics of hydrophobic drugs due to high complexing efficiency resulting in an excellent pharmacological effect of the inclusion complexes obtained. In addition, the product obtained has

amorphous characteristics as observed in Figure 7. This method can produce a good yield of inclusion complex and it is possible to scale up. Additionally, it has been widely used for thermolabile compounds, such as terpenes.<sup>49–52</sup> The yield observed for this complex was 66.22%, lower than that obtained by KN, which obtained the highest yield (86.85%).

Due to the simplicity and high yield, the KN technique has been widely used. However, its efficiency of complexation may be inferior to that achieved with other techniques.<sup>53</sup> Menezes et

al.,<sup>48</sup> for example, demonstrated a partial complexation of the monoterpene linalool by the KN method. In the DSC studies, this system demonstrated a thermal profile similar to PM and thus the possibility of a less complexation for this system was emphasized.

The complex obtained by ROE in the DSC curve presented a possibility of greater complexation in relation to KN. However, it presented a lower yield (63.98%) besides the need for strict temperature control to avoid the possibility of volatilization of this terpene during drying. Due to these reasons and other characterization studies, such as H NMR spectroscopy, the LPh system was chosen as the most promising system for future use in solid dosage forms. However, new studies may in the future still explore the system obtained by ROE because it presented similar results to LPh in the characterization studies by FTIR and DSC.

**In Vivo Pharmacological Studies.** Several studies have demonstrated the pharmaceutical or pharmacological benefits of a CD inclusion complex with natural products, and the complexation BCP/ $\beta$ CD previously showed to improve the oral bioavailability and the pharmacokinetics of free BCP after a single oral dose of 50 mg/kg on rats.<sup>28</sup> Thus, we assessed the pharmacological activity of BCP/ $M\beta$ CD orally (50 mg/kg, using a solution obtained with the Lph system) in classic animal models.

**Effect of BCP and BCP/ $M\beta$ CD on Carrageenan-Induced Paw Edema in Mice.** The anti-inflammatory potential of the inclusion complex was evaluated using a classic pharmacological model of carrageenan-induced paw edema in mice (Figure 8A). This model shows a progression of a biphasic inflammation. The first one is characterized by cellular infiltrate with predominance of polymorphonuclear (PMN) neutrophils. These cells amplify the inflammatory response via production of reactive oxygen species (ROS) and via inflammatory mediators. The second phase (24 h after induction of edema) is characterized by the intense accumulation of cells such as macrophages, eosinophils, and lymphocytes.<sup>54,55</sup>

The present experiments confirmed the anti-inflammatory effect of BCP 50 mg/kg in the first phase of carrageenan-induced paw edema. Also, BCP was able to reduce the edema by 55.8% during its peak (third hour), which is in agreement with the results previously obtained in rats by Fernandes et al.;<sup>13</sup> this inhibition is similar to the positive control (indomethacin reduction -61.04%). In turn, the inclusion complex further reduced the edema by 84%, demonstrating that the inclusion complex clearly improves the anti-inflammatory activity (Figure 8A).

Histological sections of tissue from the paw edema were observed for inflammatory markers. High infiltration damage due to accumulation of polymorphonuclear (PMN) cells and collection of fluid was seen in the carrageenan control (Figure 8B panel b, infiltrate of inflammatory cells indicated by arrowhead and edema indicated by pentagon). Biopsies of paw of animals treated with BCP (panel c) and BCP/ $M\beta$ CD (panel d) (50 mg/kg) indicated a reduction in carrageenan-induced inflammatory response similar to the indomethacin group (panel e), confirming its anti-inflammatory activity.

The neutrophil-specific enzyme myeloperoxidase (MPO), which is an indicator of neutrophil migration into the inflammatory site and has been found in neutrophil azurophilic granules, was investigated in tissue homogenates of the paws submitted to edema, as shown in Figure 9a. This enzyme activity was increased by carrageenan (Figure 9a;  $12.9 \pm 1$

UMPO/mg of tissue), whereas the groups treated with BCP and BCP/ $M\beta$ CD showed a considerable inhibition of MPO activity ( $2.6 \pm 0.9$  and  $5.1 \pm 1.3$  UMPO/mg of tissue, respectively), which was similar to the reduction in the action of this tissue enzyme by indomethacin ( $3.9 \pm 0.6$ ). Because MPO activity levels in BCP- and BCP/ $M\beta$ CD-treated animals were lower than those of Sal\* animals, it is possible to note that their anti-inflammatory activity involves the inhibition of neutrophil migration to the site of the inflammation.

**Anti-Inflammatory Effects of BCP and BCP/ $M\beta$ CD on Carrageenan-Induced Peritonitis in Mice.** To further investigate the anti-inflammatory activity previously demonstrated, carrageenan peritonitis was induced in mice to evaluate its modulatory action under the infiltrate of defense cells and antioxidant action (Figure 9). Carrageenan administration into the peritoneal cavity promoted an increase in the counts of leukocytes ( $(36 \pm 1.9) \times 10^6$  cells/mL) and neutrophils ( $(15.3 \pm 0.5) \times 10^6$  cells/mL) ( $p < 0.05$ ) (Figure 9b,c) in the peritoneal fluid. However, pretreatment with BCP and BCP/ $M\beta$ CD revealed significantly reduced leukocyte migration into the peritoneal cavity ( $(15.8 \pm 2.8) \times 10^6$ ;  $(16 \times \pm 3) \times 10^6$  cells/mL), and the same dose also considerably decreased the neutrophil count ( $(11 \pm 1.2) \times 10^6$ ;  $(10.3 \pm 0.4) \times 10^6$  cells/mL,  $p < 0.05$ ). We note that the oral treatment with natural products with high content of BCP, such as copaiba oil, also inhibited total leukocyte and neutrophil accumulation.<sup>2</sup>

**Antioxidant Effect of BCP and BCP/ $M\beta$ CD on Carrageenan-Induced Peritonitis in Mice.** Reactive oxygen species have been proposed to play an important role in the pathogenesis of inflammation and to highlight the antioxidant properties of the obtained complex evaluated by the levels of malonyldehyde, nitrite, and reduced glutathione. Figure 9a' indicates that the injection of carrageenan into the peritoneal cavity significantly increased MDA levels ( $8.7 \pm 0.6$  nmol/mL) compared to the saline-treated group ( $3.8 \pm 0.6$  nmol/mL). On the other hand, the groups pretreated with BCP and BCP/ $M\beta$ CD presented significantly reduced MDA levels ( $1.2 \pm 0.1$  and  $1.5 \pm 0.5$  nmol/g tissue, respectively,  $p < 0.05$ ) compared to the carrageenan and saline-treated groups, evidencing the good antioxidant activity of BCP and BCP inclusion complex.

The injection of carrageenan into the peritoneal cavity also showed significantly increased Nox levels ( $0.83 \pm 0.02$  nmol/mL) (Figure 9b') relative to the saline-treated group ( $0.30 \pm 0.06$  nmol/mL). The group pretreated with BCP and BCP/ $M\beta$ CD displayed significantly reduced Nox levels ( $0.19 \pm 0.006$  and  $0.23 \pm 0.06$  nmol/g tissue, respectively) compared to the carrageenan group (Sal\*) and the saline-treated group, again evidencing the good antioxidant action of BCP and BCP/ $M\beta$ CD. This action is comparable to that obtained in the indomethacin group ( $0.13 \pm 0.007$ ;  $p < 0.05$ , Figure 9). Furthermore, treatment with carrageenan ( $34 \pm 8.5$  mg/g tissue) produces a lower content of glutathione than the saline group ( $98.3 \pm 16.4$  mg/g tissue; see Figure 9c'). Pretreatment with complexed BCP (BCP/ $M\beta$ CD) significantly increased ( $94.4 \pm 7.6$  mg/g tissue) glutathione levels to values similar to the group that did not receive carrageenan. Because treatment with free BCP in solution could not restore GSH levels, this sesquiterpene clearly presented better results in the complexed form.

These results confirm the previous findings on BCP, reporting chain-breaking antioxidant activity and ability to scavenge ROS in different tissues.<sup>4,56,57</sup> The present study demonstrated that the inclusion complex could be a way to

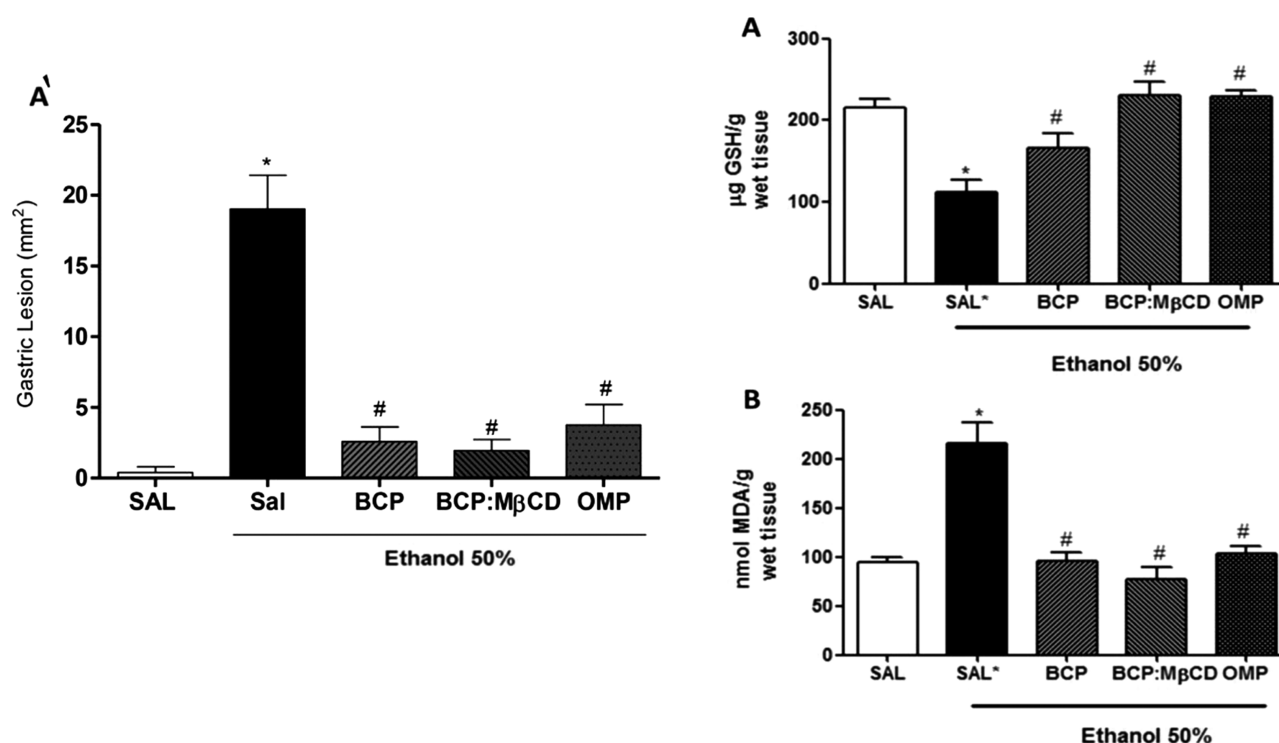


**Figure 10.** (A') Macroscopic analysis of the gastric lesions induced by ethanol pretreated with BCP and BCP/MβCD. (A) Effects of BCP and BCP/MβCD (50 mg/kg) on GSH levels in gastric damage. (B) Effects of BCP and BCP/MβCD (50 mg/kg) on MDA concentrations in gastric damage. Data are presented as mean ± SEM of five mice per group. Results were analyzed by analysis of variance, followed by Newman–Keuls post hoc test.

orally deliver the insoluble sesquiterpene BCP and at the same time to improve the respective properties.

**Prevention of Ethanol-Induced Gastric Damage by BCP and BCP/MβCD.** Among the interesting properties related to BCP, its anti-inflammatory action was shown to be devoid of associated gastric damage, demonstrating, on the other hand, to exert gastric and cytoprotective anti-inflammatory effects on the gastrointestinal tract.<sup>12,17</sup> In this regard, the gastric protective effects of the inclusion complex obtained (Figure 10) were evaluated.

Our results showed that treatment of mice with ethanol led to severe macroscopic gastric damage characterized by intense hemorrhage ( $19.0 \pm 2.4$  mm<sup>2</sup>), in agreement with the already described findings.<sup>58–61</sup> Interestingly, pretreatment with BCP and BCP/MβCD in aqueous solution prevented ethanol-induced macroscopic damage, to an extent similar to that found in the omeprazol (OMP)-treated group (Figure 10A',  $2.6 \pm 1$  and  $2.0 \pm 0.8$  mm<sup>2</sup>, respectively,  $p < 0.005$ ). The pathogenesis of gastric mucosal damage induced by ethanol is a multifactorial process involving an increase in aggressive factors, such as ROS generation and a decrease in endogenous defense mechanisms.<sup>61</sup>

**Antioxidant Effect of BCP and BCP/MβCD on Ethanol-Induced Gastric Damage.** It has been suggested that oxygen-derived free radicals (ROS) is the main factor that contributes to ethanol-induced gastric mucosal lesions.<sup>62,63</sup> This effect in gastric mucosa by ROS is mediated by lipid peroxidation. It was also demonstrated that ethanol reduces GSH and glutathione peroxidase activity.<sup>59,64</sup>

Treatment with 50% of ethanol significantly decreased GSH concentrations ( $112.4 \pm 15.1$  mg/g tissue) and increased MDA levels ( $205.2 \pm 21.5$  nmol/g tissue) compared to the control group ( $p < 0.05$ ; Figure 10). Pretreatment with BCP (50 mg/

kg) and BCP/MβCD (50 mg/kg) in aqueous solution increased the levels of the endogenous antioxidant GSH ( $166.3 \pm 17.6$  and  $231.1 \pm 16.3$  mg/g tissue, respectively), restoring the damage caused by ethanol (Figure 10A), and BCP/MβCD exhibited a significantly better ( $p < 0.05$ ) effect than BCP. The administration of BCP (50 mg/kg) and BCP/MβCD (50 mg/kg) ( $96.4 \pm 8$  and  $77.2 \pm 11.78$  nmol/g tissue, respectively) also significantly reduced the concentration of gastric mucosal MDA induced by ethanol (Figure 10B).

In a previous study, BCP is demonstrated to exert protective effects on the gastric mucosa with suppression of ulcerogenesis in doses from 25 mg/kg orally, without affecting gastric acid secretion. Its action is suggested potentiating defensive mucosal factors.<sup>12</sup> This study shows based on GSH and MDA levels that BCP/MβCD also has protective effects on gastric mucosa and that this effect seems to involve the reduction of lipid peroxidation induced by ethanol instillation.

Several studies have shown that complexation of standard drugs or active natural products in cyclodextrins can improve their biological effects.<sup>65,66</sup> Here, we demonstrated that the BCP/MβCD inclusion complex can be a useful drug-delivery system to improve the pharmacological activity of BCP and could be a strategy to circumvent the technical features that have limited its therapeutic use.

## CONCLUSIONS

We have formulated a novel inclusion complex with BCP in MβCD that can lead to important modifications on the solubility of the guest. Information obtained from DSC, SEM, and <sup>1</sup>H NMR studies show that stable solid BCP/MβCD inclusion complexes can be prepared at a 1:1 molar ratio by KN, ROE, and LPh methods. The LPh system has been shown to be more promising for future use in solid dosage forms. Data

from  $^1\text{H}$  NMR and ROESY spectra demonstrate that complexation occurs preferentially by the doubly methylated part of BCP, and molecular dynamics simulation studies showed the possibility of two kinds of inclusion of the BCP. In both cases, the drug molecule stays preferentially closer to the wider portal of the CD cavity. Moreover, this inclusion complex promotes an improvement of the anti-inflammatory, gastric protection and antioxidant activities relative to neat BCP. Therefore, BCP/ $M\beta\text{CD}$  can be a useful new drug-delivery system to BCP molecule and could be one solution to technical features that have limited the therapeutic use of this active natural product.

## EXPERIMENTAL SECTION

**Phase Solubility Studies.** Phase solubility studies were performed using  $M\beta\text{CD}$  and  $HP\beta\text{CD}$  following the method described by Higuchi and Connors.<sup>31</sup> For this purpose, an excess of BCP was added to the flask containing increased concentrations (0–40 mM) of  $M\beta\text{CD}$  or  $HP\beta\text{CD}$  in aqueous solution. The samples were kept under agitation for 72 h until equilibrium. After that, aliquots were taken, filtered with membrane filters (0.45  $\mu\text{m}$ ), diluted in a solution of ethanol/water (1:9, v/v), centrifuged for 10 min, and analyzed spectrophotometrically (Shimadzu UV 1800) at 203 nm.<sup>28,67</sup> The experiments were conducted in triplicate. The apparent stability constants ( $K_s$ ) were calculated with the data obtained from the following equation

$$K_s = \text{slope}/S_0 \times (1 - \text{slope})$$

where  $S_0$  represents the intrinsic solubility of the  $\beta$ -caryophyllene.

**Preparation of the Inclusion Complexes in the Solid State.** According to the phase solubility results, solid systems were prepared in an equimolar ratio between BCP and  $M\beta\text{CD}$ . Three distinct methods were used: KN, ROE, and LPH. The physical mixture (PM) between BCP and  $M\beta\text{CD}$  was also prepared and used as reference. PM was prepared by simply blending BCP and  $M\beta\text{CD}$  with 1:1 molar ratio uniformly in a mortar. The KN, ROE, and LPH were prepared according to the methodology already described by de Freitas et al.<sup>23</sup> and Santos et al.<sup>68</sup> with some modifications. CD was previously sieved (180  $\mu\text{m}$  sieve granulometric fraction). The final products were hermetically stored in a closed amber glass.

**Characterization of the Prepared Inclusion Complexes.** *Fourier Transform Infrared (FTIR) Spectroscopy.* FTIR analyses were performed in a JASCO FT/IR-420 spectrometer associated with horizontal reflection attenuated total reflection (MIRacle, PIKE Technologies). The spectra were obtained in the region of the IR (4000–400  $\text{cm}^{-1}$ ) with the application of 16 scans at a resolution of 4  $\text{cm}^{-1}$ .

*Differential Scanning Calorimetry (DSC).* Thermal analyses of raw materials and prepared systems were carried out using a differential scanning calorimeter (Shimadzu 60 series) associated to a thermic analyzer linked to the software Shimadzu TA-60WS/PC. The analyses were made in an atmosphere of nitrogen with a flux of 20  $\text{cm}^3/\text{min}$  under a heat ratio of 10  $^\circ\text{C}/\text{min}$  from 25 to 250  $^\circ\text{C}$ . For this purpose, sealed aluminum pans were used. An empty pan was used as reference. Indio (99.98%, 156.65  $^\circ\text{C}$ , Aldrich, Milwaukee) was used as standard for the calibration of the temperature.

*Scanning Electronic Microscopy (SEM).* The surface morphology of  $M\beta\text{CD}$  and binary systems was examined and photographed using a scanning electron microscope (JSM

6010-LC, JEOL, Tokyo, Japan). The samples were fixed in surfaces of double-sided tape, and further, a coating with a thin layer of gold was made due to the nonconductivity of samples. Photographs were taken at an excitation voltage of 10 kV and a magnification factor of 1000 $\times$ .

*$^1\text{H}$  NMR Spectroscopy.*  $^1\text{H}$  NMR spectra of BCP,  $M\beta\text{CD}$ , and the LPH binary system were acquired on a Varian 600 MHz spectrometer using a 3 mm indirect detection NMR probe and deuterated dimethyl sulfoxide ( $\text{DMSO}-d_6$ ) as solvent. Acquisition parameters consisted of 43k points covering a sweep width of 7.2 kHz, a pulse width of 2.4  $\mu\text{s}$ , equivalent to a 45 $^\circ$  pulse angle, and a total repetition time of 10 s.  $^1\text{H}$  NMR chemical shift variations ( $\Delta\delta$ ) were calculated according to the formula

$$\Delta\delta = \delta(\text{complex}) - \delta(\text{free})$$

*ROESY Spectroscopy.* The extent and the direction of the inclusion in the CD cavity were determined by two-dimensional phase-sensitive nuclear Overhauser effect (NOE) spectroscopy by the detection of intermolecular nuclear Overhauser effects (NOEs) between BCP and  $M\beta\text{CD}$ . ROESY spectra were acquired in the phase-sensitive mode using the same spectrometer and probe. Acquisition parameters included 1.7k and 0.9k in F2 and F1 dimensions, respectively, defining a spectral width of 5 kHz. Before Fourier transform, the FID was zero-filled and multiplied by a Gaussian apodization function in both dimensions. The magnetization mixing period chosen was 150 ms, after calibration.

*Molecular Dynamics Simulation.* MD simulations were carried out using the Gromacs package, version 4.5.5,<sup>69</sup> and the GROMOS 53a6 force field was applied.<sup>70</sup> The structure of  $M\beta\text{CD}$  was constructed from  $\beta\text{CD}$  (obtained from the HIC-Up online database), in which the methyl groups were introduced to achieve the appropriate substitution degree of the CD used experimentally.<sup>71–73</sup> The topologies for  $M\beta\text{CD}$  and BCP molecule structure were obtained by the ATB server.<sup>74</sup>

The two molecules were immersed in cubic boxes filled with necessary water molecules. The SPC216 water model was used for the solvent molecules. MD simulations were carried out in the NpT ensemble and under periodic boundary conditions, at a constant pressure (1 bar) and constant temperature (298 K) coupled, respectively, to v-rescale and Berendsen external baths. A standard time step of 2 fs was used for both equilibration and production runs. Nonbonded interactions were computed on the basis of a neighbor list, updated every 10 steps.

The long-range electrostatic interactions were treated based on the particle mesh Ewald method.<sup>75</sup> A cutoff of 1.2 nm was applied for the Lennard-Jones energies. Initial energy minimization was performed for the system and then a production run of 100 ns using the LINCS algorithm.<sup>76,77</sup> The last 60 ns were subjected to the standard analysis. The formation of the inclusion complex was a result of an equilibration process in vacuum, which was only considered to be completed when inclusion was visualized. The trajectories of the host–guest molecules interactions were saved and analyzed. The configuration images were produced using the software VMD 1.9.

**Animals.** Mice (Swiss, 25–30 g) of both sexes were used. They were maintained in a room with controlled temperature (22  $\pm$  1  $^\circ\text{C}$ ) under a 12 h light/12 h dark cycle for at least a week before being used (five to six animals per group). The animals had water ad libitum and a standard pellet diet. The care of laboratory animals was performed in accordance with

the Guide for Care and Use of Laboratory Animals (National Institutes of Health) and was approved by the local ethics committee (Protocol No. 0002/15).

**Drug Administration.** Equivalent volumes of test drugs or vehicle were administered in separate groups ( $n = 5$ ) of mice prior to inducing them to the pharmacological models. In separate experiments, were injected intraperitoneally (ip) saline solution 0.9% as untreated control (Sal\*), indomethacin (INDO) as standard anti-inflammatory drug 10 mg/kg, and omeprazol (OMP) as standard gastric protect drug 10 mg/kg given in saline. The BCP was dissolved in water to obtain a solution of the same content of BCP in a solution obtained by dissolving the solid inclusion complex obtained by the LPh system. These solutions were administered orally in separated groups described by BCP 50 mg/kg (BCP) or BCP/M $\beta$ CD 50 mg/kg (BCP/M $\beta$ CD). The negative group received an injection of 0.9% sterile saline (Sal).

**Carrageenan-Induced Paw Edema Test.** Carrageenan-induced paw edema test was carried out as previously described.<sup>54</sup> After 1 h treatments of tested drugs (Sal\*, INDO, BCP, and BCP/M $\beta$ CD) edema was induced by intraplantar injection of 50  $\mu$ L of a carrageenan suspension (500  $\mu$ g/paw) in 0.9% sterile saline. The negative (Sal) group received an injection of 50  $\mu$ L of 0.9% sterile saline only. Paw volume was measured immediately after the induction ( $V_o$ ) and 1, 2, 3, and 4 h after carrageenan treatment ( $V_t$ ) using a plethysmometer (LE 7500, Panlab, Barcelona, Spain). The effect of pretreatment was calculated as percent inhibition of edema relative to the paw volume of the untreated control using the following formula

$$\text{inhibition (\%)} = \frac{(V_t - V_o)\text{control} - (V_t - V_o)\text{treatment}}{(V_t - V_o)\text{control}} \times 100$$

**Histological Analysis.** To evaluate the degree of inflammation, all groups submitted to carrageenan-induced paw edema tests underwent histopathological analysis. Paw biopsies were taken 4 h after carrageenan administration. Tissue slices were fixed in 10% buffered formaldehyde for 24 h, dehydrated in ethanol 70%, embedded in paraffin, and sectioned (5  $\mu$ m). The sections were stained with hematoxylin–eosin and examined under a light microscope analysis.

**Assessment of Myeloperoxidase (MPO) Activity.** MPO activity in paw tissues was measured by the method described by Bradley et al.<sup>78</sup> Paw tissues (50 mg) were crushed in hexadecyltrimethylammonium buffer (pH 6) using a tissue homogenizer and centrifuged at 4500 rpm (12 min at 4 °C). The supernatant was collected to react with a solution of 1% hydrogen peroxide. The optical density change of the samples following the addition of *o*-dianisidine was measured by a spectrophotometer (450 nm) as a function of reaction time. MPO activity was defined as the quantity of enzyme degrading 1  $\mu$ mol of hydrogen peroxide per minute at 22 °C and was expressed in units of MPO (UMPO)/mg tissue.<sup>78</sup>

**Carrageenan-Induced Peritonitis Test.** Carrageenan-induced peritonitis test was carried out as previously described by administrating 250  $\mu$ L of a carrageenan suspension (500  $\mu$ g/cavity, ip) 1 h after the pretreatment with Sal\*, INDO, BCP, or BCP/M $\beta$ CD. After 4 h, the animals were euthanized and the peritoneal cavity was washed with 1.5 mL of heparinized phosphate-buffered saline, to obtain peritoneal cells. Total cell count was determined using a Neubauer chamber. The

differential 100 cell count was performed in slides prepared using a cytocentrifuge, stained with hematoxylin and eosin, and examined with an optical microscope for neutrophil migration. Aliquots of the peritoneal exudates were stored at  $-70$  °C for later analysis. The reduced glutathione (GSH) content in the exudate was estimated according to the method described by Sedlak and Lindsay,<sup>79</sup> the content of malondialdehyde (MDA) was measured by the method of Mihara and Uchiyama,<sup>80</sup> and nitrite content was determined as previously described by Prado et al.<sup>81</sup>

**Effects of BCP and BCP/M $\beta$ CD on Ethanol-Induced Gastric Damage.** The animals were deprived of food for 18–24 h before the experiments, but had free access to water and were initially pretreated with Sal\*, BCP, BCP/M $\beta$ CD, or OMP. After 1 h, ethanol 50% (0.5 mL/25 g) was administered by gavage. One hour after ethanol ingestion, the mice were euthanized and stomach samples were collected for biochemical analysis and macroscopic evaluations of gastric mucosa. Gastric damage was measured using a computer planimetry program (ImageJ software; National Institutes of Health, Bethesda, MD).<sup>58</sup> Reduced GSH content in stomach samples as nonprotein sulfhydryls was estimated according to the method described by Sedlak and Lindsay,<sup>79</sup> and malondialdehyde (MDA) assay was measured using the method of Mihara and Uchiyama.<sup>80</sup>

## ■ ASSOCIATED CONTENT

### 📄 Supporting Information

The Supporting Information is available free of charge on the ACS Publications website at DOI: 10.1021/acsomega.7b01438.

Methods of preparation of the inclusion complexes in the solid state and the correlation spectroscopy spectrum obtained to confirm attributions of the <sup>1</sup>H resonances of BCP protons (PDF)

## ■ AUTHOR INFORMATION

### Corresponding Author

\*E-mail: rfigueiras@ff.uc.pt. Phone: + 351 239 488 400. Fax: + 351 239 488 503. Faculty of Pharmacy, University of Coimbra, Pólo das Ciências da Saúde, Azinhaga de Santa Comba, 3000-548 Coimbra, Portugal.

### ORCID

Ana Figueiras: 0000-0001-8170-1113

### Funding

This work was supported by Coordination for the Improvement of Higher Education Personnel (CAPES) (Coordenação de Aperfeiçoamento de Pessoal de Nível Superior—CAPES), Brazil (research scholarship—“doutorado sanduíche” program of mobility); Fundação para a Ciência e Tecnologia (FCT), Portugal (post-doctoral grant SFRH/BPD/71683/2010); and CQC (project no. 007630 UID/QUI/00313/2013, co-funded by COMPETE2020-UE).

### Notes

The authors declare no competing financial interest.

## ■ REFERENCES

- (1) Cho, H.-I.; Hong, J.-M.; Choi, J.-W.; Choi, H.-S.; Kwak, J. H.; Lee, D.-U.; Lee, S. K.; Lee, S.-M.  $\beta$ -Caryophyllene alleviates d-galactosamine and lipopolysaccharide-induced hepatic injury through suppression of the TLR4 and RAGE signaling pathways. *Eur. J. Pharmacol.* **2015**, *764*, 613–621.

- (2) Leandro, L. M.; de Sousa Vargas, F.; Barbosa, P. C. S.; Neves, J. K. O.; da Silva, J. A.; da Veiga-Junior, V. F. Chemistry and Biological Activities of Terpenoids from Copaiba (*Copaifera* spp.) Oleoresins. *Molecules* **2012**, *17*, 3866–3889.
- (3) Yang, Y.-C.; Wei, M.-C.; Hong, S.-J. Ultrasound-assisted extraction and quantitation of oils from *Syzygium aromaticum* flower bud (clove) with supercritical carbon dioxide. *J. Chromatogr. A* **2014**, *1323*, 18–27.
- (4) Calleja, M. A.; Vieites, J. M.; Montero-Meterdez, T.; Torres, M. I.; Faus, M. J.; Gil, A.; Suárez, A. The antioxidant effect of  $\beta$ -caryophyllene protects rat liver from carbon tetrachloride-induced fibrosis by inhibiting hepatic stellate cell activation. *Br. J. Nutr.* **2013**, *109*, 394–401.
- (5) Pant, A.; Saikia, S. K.; Shukla, V.; Asthana, J.; Akhooon, B. A.; Pandey, R. Beta-caryophyllene modulates expression of stress response genes and mediates longevity in *Caenorhabditis elegans*. *Exp. Gerontol.* **2014**, *57*, 81–95.
- (6) Klauke, A.-L.; Racz, I.; Pradier, B.; Markert, A.; Zimmer, A. M.; Gertsch, J.; Zimmer, A. The cannabinoid CB2 receptor-selective phytocannabinoid beta-caryophyllene exerts analgesic effects in mouse models of inflammatory and neuropathic pain. *Eur. Neuropsychopharmacol.* **2014**, *24*, 608–620.
- (7) Park, K.-R.; Nam, D.; Yun, H.-M.; Lee, S.-G.; Jang, H.-J.; Sethi, G.; Cho, S. K.; Ahn, K. S.  $\beta$ -Caryophyllene oxide inhibits growth and induces apoptosis through the suppression of PI3K/AKT/mTOR/S6K1 pathways and ROS-mediated MAPKs activation. *Cancer Lett.* **2011**, *312*, 178–188.
- (8) Dahham, S. S.; Tabana, Y. M.; Iqbal, M. A.; Ahamed, M. B. K.; Ezzat, M. O.; Majid, A. S. A.; Majid, A. M. S. A. The Anticancer, Antioxidant and Antimicrobial Properties of the Sesquiterpene  $\beta$ -Caryophyllene from the Essential Oil of *Aquilaria crassna*. *Molecules* **2015**, *20*, 11808–11829.
- (9) Bahi, A.; Al Mansouri, S.; Al Memari, E.; Al Ameri, M.; Nurulain, S. M.; Ojha, S.  $\beta$ -Caryophyllene, a CB2 receptor agonist produces multiple behavioral changes relevant to anxiety and depression in mice. *Physiol. Behav.* **2014**, *135*, 119–124.
- (10) Horváth, B.; Mukhopadhyay, P.; Kechrid, M.; Patel, V.; Tanchian, G.; Wink, D. A.; Gertsch, J.; Pacher, P.  $\beta$ -Caryophyllene ameliorates cisplatin-induced nephrotoxicity in a cannabinoid 2 receptor-dependent manner. *Free Radical Biol. Med.* **2012**, *52*, 1325–1333.
- (11) Chang, H.-J.; Kim, J.-M.; Lee, J.-C.; Kim, W.-K.; Chun, H. S. Protective Effect of  $\beta$ -Caryophyllene, a Natural Bicyclic Sesquiterpene, Against Cerebral Ischemic Injury. *J. Med. Food* **2013**, *16*, 471–480.
- (12) Tambe, Y.; Tsujiuchi, H.; Honda, G.; Ikeshiro, Y.; Tanaka, S. Gastric Cytoprotection of the Non-Steroidal Anti-Inflammatory Sesquiterpene,  $\beta$ -Caryophyllene. *Planta Med.* **1996**, *62*, 469–470.
- (13) Fernandes, E. S.; Passos, G. F.; Medeiros, R.; da Cunha, F. M.; Ferreira, J.; Campos, M. M.; Pianowski, L. F.; Calixto, J. B. Anti-inflammatory effects of compounds alpha-humulene and (–)-trans-caryophyllene isolated from the essential oil of *Cordia verbenacea*. *Eur. J. Pharmacol.* **2007**, *569*, 228–236.
- (14) Veiga, V. F.; Rosas, E. C.; Carvalho, M. V.; Henriques, M. G. M. O.; Pinto, A. C. Chemical composition and anti-inflammatory activity of copaiba oils from *Copaifera cearensis* Huber ex Ducke, *Copaifera reticulata* Ducke and *Copaifera multijuga* Hayne—A comparative study. *J. Ethnopharmacol.* **2007**, *112*, 248–254.
- (15) Paula-Freire, L. I. G.; Andersen, M. L.; Gama, V. S.; Molska, G. R.; Carlini, E. L. A. The oral administration of trans-caryophyllene attenuates acute and chronic pain in mice. *Phytomedicine* **2014**, *21*, 356–362.
- (16) Quintans-Júnior, L. J.; Araújo, A. A. S.; Brito, R. G.; Santos, P. L.; Quintans, J. S. S.; Menezes, P. P.; Serafini, M. R.; Silva, G. F.; Carvalho, F. M. S.; Brogden, N. K.; et al.  $\beta$ -Caryophyllene, a dietary cannabinoid, complexed with  $\beta$ -cyclodextrin produced anti-hyperalgesic effect involving the inhibition of Fos expression in superficial dorsal horn. *Life Sci.* **2016**, *149*, 34–41.
- (17) Bento, A. F.; Marcon, R.; Dutra, R. C.; Claudino, R. F.; Cola, M.; Leite, D. F. P.; Calixto, J. B.  $\beta$ -Caryophyllene Inhibits Dextran Sulfate Sodium-Induced Colitis in Mice through CB2 Receptor Activation and PPAR $\gamma$  Pathway. *Am. J. Pathol.* **2011**, *178*, 1153–1166.
- (18) Gertsch, J.; Leonti, M.; Raduner, S.; Racz, I.; Chen, J.-Z.; Xie, X.-Q.; Altmann, K.-H.; Karsak, M.; Zimmer, A. Beta-caryophyllene is a dietary cannabinoid. *Proc. Natl. Acad. Sci. U.S.A.* **2008**, *105*, 9099–9104.
- (19) Sarpietro, M. G.; Di Sotto, A.; Accolla, M. L.; Castelli, F. Interaction of  $\beta$ -caryophyllene and  $\beta$ -caryophyllene oxide with phospholipid bilayers: Differential scanning calorimetry study. *Thermochim. Acta* **2015**, *600*, 28–34.
- (20) Sköld, M.; Karlberg, A.-T.; Matura, M.; Börje, A. The fragrance chemical  $\beta$ -caryophyllene—air oxidation and skin sensitization. *Food Chem. Toxicol.* **2006**, *44*, 538–545.
- (21) Siqueira-Lima, P. S.; Araújo, A. A. S.; Lucchese, A. M.; Quintans, J. S. S.; Menezes, P. P.; Alves, P. B.; de Lucca Júnior, W.; Santos, M. R. V.; Bonjardim, L. R.; Quintans-Júnior, L. J.  $\beta$ -Cyclodextrin Complex Containing *Lippia grata* Leaf Essential Oil Reduces Orofacial Nociception in Mice – Evidence of Possible Involvement of Descending Inhibitory Pain Modulation Pathway. *Basic Clin. Pharmacol. Toxicol.* **2014**, *114*, 188–196.
- (22) Menezes, P. P.; Serafini, M. R.; Santana, B. V.; Nunes, R. S.; Quintans, L. J.; Silva, G. F.; Medeiros, I. A.; Marchioro, M.; Fraga, B. P.; Santos, M. R. V.; et al. Solid-state  $\beta$ -cyclodextrin complexes containing geraniol. *Thermochim. Acta* **2012**, *548*, 45–50.
- (23) de Freitas, M. R.; Rolim, L. A.; de La Roca Soares, M. F.; Rolim-Neto, P. J.; de Albuquerque, M. M.; Soares-Sobrinho, J. L. Inclusion complex of methyl- $\beta$ -cyclodextrin and olanzapine as potential drug delivery system for schizophrenia. *Carbohydr. Polym.* **2012**, *89*, 1095–1100.
- (24) Ciobanu, A.; Mallard, I.; Landy, D.; Brabie, G.; Nistor, D.; Fourmentin, S. Inclusion interactions of cyclodextrins and crosslinked cyclodextrin polymers with linalool and camphor in *Lavandula angustifolia* essential oil. *Carbohydr. Polym.* **2012**, *87*, 1963–1970.
- (25) Fang, Z.; Comino, P. R.; Bhandari, B. Effect of encapsulation of d-limonene on the moisture adsorption property of  $\beta$ -cyclodextrin. *LWT – Food Sci. Technol.* **2013**, *51*, 164–169.
- (26) dos Santos, C.; del Pilar Buera, M.; Mazzobre, M. F. Phase solubility studies of terpineol with  $\beta$ -cyclodextrins and stability of the freeze-dried inclusion complex. *Procedia Food Sci.* **2011**, *1*, 355–362.
- (27) Santos, P. L.; Brito, R. G.; Oliveira, M. A.; Quintans, J. S. S.; Guimarães, A. G.; Santos, M. R. V.; Menezes, P. P.; Serafini, M. R.; Menezes, I. R. A.; Coutinho, H. D. M.; et al. Docking, characterization and investigation of  $\beta$ -cyclodextrin complexed with citronellal, a monoterpene present in the essential oil of *Cymbopogon* species, as an anti-hyperalgesic agent in chronic muscle pain model. *Phytomedicine* **2016**, *23*, 948–957.
- (28) Liu, H.; Yang, G.; Tang, Y.; Cao, D.; Qi, T.; Qi, Y.; Fan, G. Physicochemical characterization and pharmacokinetics evaluation of  $\beta$ -caryophyllene/ $\beta$ -cyclodextrin inclusion complex. *Int. J. Pharm.* **2013**, *450*, 304–310.
- (29) Menezes, P. P.; Araujo, A. A.; Doria, G. A.; Quintans-Junior, L. J.; Oliveira, J. F.; Matos, J. R.; Carvalho, F. M.; Alves, P. B.; Matos, I. L.; Santos, D. A.; Marreto, R. N.; Silva, G. F.; Serafini, M. R. Physicochemical characterization and analgesic effect of inclusion complexes of essential oil from *Hyptis pectinata* L. poit leaves with  $\beta$ -cyclodextrin. *Curr. Pharm. Biotechnol.* **2015**, *16*, 440–450.
- (30) Rakmai, J.; Cheirsilp, B.; Mejuto, J. C.; Torrado-Agrasar, A.; Simal-Gándara, J. Physico-chemical characterization and evaluation of bio-efficacies of black pepper essential oil encapsulated in hydroxypropyl-beta-cyclodextrin. *Food Hydrocolloids* **2017**, *65*, 157–164.
- (31) Higuchi, T.; Connors, K. A. Phase-Solubility Techniques. In *Advances in Analytical Chemistry and Instrumentation*; Reilly, C. N., Ed.; Wiley-Interscience, 1965; Vol. 4, pp 117–212.
- (32) Mura, P. Analytical techniques for characterization of cyclodextrin complexes in aqueous solution: A review. *J. Pharm. Biomed. Anal.* **2014**, *101*, 238–250.
- (33) Veiga, F.; Pecorelli, C.; Ribeiro, L. *As ciclodextrinas em tecnologia farmacêutica*; Minerva Coimbra, 2006.

- (34) Lyra, M. A. M.; Alves, L. D. S.; Fontes, D. A. F.; Soares-Sobrinho, J. L.; Rolim-Neto, P. J. Ferramentas analíticas aplicadas à caracterização de complexos de inclusão fármaco-ciclodextrina. *Rev. Cienc. Farm. Basica Apl.* **2010**, *31*, 117–124.
- (35) de Miranda, J. C.; Martins, T. E. A.; Veiga, F.; Ferraz, H. G. Cyclodextrins and ternary complexes: technology to improve solubility of poorly soluble drugs. *Braz. J. Pharm. Sci.* **2011**, *47*, 665–681.
- (36) Mukne, A. P.; Nagarsenker, M. S. Triamterene-beta-cyclodextrin systems: preparation, characterization and in vivo evaluation. *AAPS PharmSciTech* **2004**, *5*, 142.
- (37) Lou, J.; Teng, Z.; Zhang, L.; Yang, J.; Ma, L.; Wang, F.; Tian, X.; An, R.; Yang, M.; Zhang, Q.  $\beta$ -caryophyllene/hydroxypropyl- $\beta$ -cyclodextrin inclusion complex improves cognitive deficits in rats with vascular dementia through the cannabinoid receptor type 2-mediated pathway. *Front. Pharmacol.* **2017**, *8*, 1–16.
- (38) Choi, S. G.; Lee, S.-E.; Kang, B.-S.; Ng, C. L.; Davaa, E.; Park, J.-S. Thermosensitive and Mucoadhesive Sol–Gel Composites of Paclitaxel/Dimethyl- $\beta$ -Cyclodextrin for Buccal Delivery. *PLoS One* **2014**, *9*, No. e109090.
- (39) Dandawate, P.; Vemuri, K.; Swamy, K. V.; Khan, E. M.; Sritharan, M.; Padhye, S. Synthesis, characterization, molecular docking and anti-tubercular activity of Plumbagin–Isoniazid Analog and its  $\beta$ -cyclodextrin conjugate. *Bioorg. Med. Chem. Lett.* **2014**, *24*, 5070–5075.
- (40) Zhou, Q.; Zhong, L.; Wei, X.; Dou, W.; Chou, G.; Wang, Z. Baicalein and hydroxypropyl- $\gamma$ -cyclodextrin complex in poloxamer thermal sensitive hydrogel for vaginal administration. *Int. J. Pharm.* **2013**, *454*, 125–134.
- (41) Figueiras, A.; Carvalho, R. A.; Ribeiro, L.; Torres-Labandeira, J. J.; Veiga, F. J. B. Solid-state characterization and dissolution profiles of the inclusion complexes of omeprazole with native and chemically modified  $\beta$ -cyclodextrin. *Eur. J. Pharm. Biopharm.* **2007**, *67*, 531–539.
- (42) Mura, P. Analytical techniques for characterization of cyclodextrin complexes in the solid state: A review. *J. Pharm. Biomed. Anal.* **2015**, *113*, 226–238.
- (43) Ma, S.-X.; Chen, W.; Yang, X.-D.; Zhang, N.; Wang, S.-J.; Liu, L.; Yang, L.-J. Alpinetin/hydroxypropyl- $\beta$ -cyclodextrin host–guest system: Preparation, characterization, inclusion mode, solubilization and stability. *J. Pharm. Biomed. Anal.* **2012**, *67*–68, 193–200.
- (44) Chen, W.; Yang, L.-J.; Ma, S.-X.; Yang, X.-D.; Fan, B.-M.; Lin, J. Crassicauline A/ $\beta$ -cyclodextrin host–guest system: Preparation, characterization, inclusion mode, solubilization and stability. *Carbohydr. Polym.* **2011**, *84*, 1321–1328.
- (45) García, A.; Leonardi, D.; Vasconi, M. D.; Hinrichsen, L. I.; Lamas, M. C. Characterization of albendazole-randomly methylated- $\beta$ -cyclodextrin inclusion complex and in vivo evaluation of its antihelminthic activity in a murine model of Trichinellosis. *PLoS One* **2014**, *9*, No. e113296.
- (46) Xu, C.; Tang, Y.; Hu, W.; Tian, R.; Jia, Y.; Deng, P.; Zhang, L. Investigation of inclusion complex of honokiol with sulfobutyl ether- $\beta$ -cyclodextrin. *Carbohydr. Polym.* **2014**, *113*, 9–15.
- (47) Periasamy, R.; Kothainayaki, S.; Rajamohan, R.; Sivakumar, K. Spectral investigation and characterization of host–guest inclusion complex of 4,4'-methylene-bis(2-chloroaniline) with beta-cyclodextrin. *Carbohydr. Polym.* **2014**, *114*, 558–566.
- (48) Menezes, P. P.; Serafini, M. R.; Quintans-Júnior, L. J.; Silva, G. F.; Oliveira, J. F.; Carvalho, F. M. S.; Souza, J. C. C.; Matos, J. R.; Alves, P. B.; Matos, I. L.; et al. Inclusion complex of (–)-linalool and  $\beta$ -cyclodextrin. *J. Therm. Anal. Calorim.* **2014**, *115*, 2429–2437.
- (49) Zhang, Y.; Meng, F.-C.; Cui, Y.-L.; Song, Y.-F. Enhancing Effect of Hydroxypropyl- $\beta$ -cyclodextrin on the Intestinal Absorption Process of Genipin. *J. Agric. Food Chem.* **2011**, *59*, 10919–10926.
- (50) Kfoury, M.; Balan, R.; Landy, D.; Nistor, D.; Fourmentin, S. Investigation of the complexation of essential oil components with cyclodextrins. *Supramol. Chem.* **2015**, *27*, 620–628.
- (51) Kfoury, M.; Auezova, L.; Fourmentin, S.; Greige-Gerges, H. Investigation of monoterpenes complexation with hydroxypropyl- $\beta$ -cyclodextrin. *J. Inclusion Phenom. Macrocyclic Chem.* **2014**, *80*, 51–60.
- (52) Mourtzinos, I.; Kalogeropoulos, N.; Papadakis, S. E.; Konstantinou, K.; Karathanos, V. T. Encapsulation of Nutraceutical Monoterpenes in  $\beta$ -Cyclodextrin and Modified Starch. *J. Food Sci.* **2008**, *73*, S89–S94.
- (53) Cunha-Filho, M. S. S.; Sá-Barreto, L. C. L. Utilização de ciclodextrinas na formação de complexos de inclusão de interesse farmacêutico. *Rev. Cienc. Farm. Basica Apl.* **2007**, *28*, 1–9.
- (54) Silva, V. G.; Silva, R. O.; Damasceno, S. R. B.; Carvalho, N. S.; Prudêncio, R. S.; Aragão, K. S.; Guimarães, M. A.; Campos, S. A.; Vêras, L. M. C.; Godejohann, M.; et al. Anti-inflammatory and Antinociceptive Activity of Epiisopiloturine, an Imidazole Alkaloid Isolated from *Pilocarpus microphyllus*. *J. Nat. Prod.* **2013**, *76*, 1071–1077.
- (55) Santiago, R. F.; de Brito, T. V.; Dias, J. M.; Dias, G. J.; da Cruz, J. S.; Batista, J. A.; Silva, R. O.; Souza, M. H. L. P.; de Albuquerque Ribeiro, R.; Gutierrez, S. J. C.; et al. Riparin B, a Synthetic Compound Analogue of Riparin, Inhibits the Systemic Inflammatory Response and Oxidative Stress in Mice. *Inflammation* **2015**, *38*, 2203–2215.
- (56) Basha, R. H.; Sankaranarayanan, C.  $\beta$ -Caryophyllene, a natural sesquiterpene lactone attenuates hyperglycemia mediated oxidative and inflammatory stress in experimental diabetic rats. *Chem.-Biol. Interact.* **2016**, *245*, 50–58.
- (57) de Oliveira, C. C.; de Oliveira, C. V.; Grigoletto, J.; Ribeiro, L. R.; Funck, V. R.; Grauncke, A. C. B.; de Souza, T. L.; Souto, N. S.; Furian, A. F.; Menezes, I. R. A.; et al. Anticonvulsant activity of  $\beta$ -caryophyllene against pentylenetetrazol-induced seizures. *Epilepsy Behav.* **2016**, *56*, 26–31.
- (58) Medeiros, J. V. R.; Bezerra, V. H.; Gomes, A. S.; Barbosa, A. L. R.; Lima-Junior, R. C. P.; Soares, P. M. G.; Brito, G. A. C.; Ribeiro, R. A.; Cunha, F. Q.; Souza, M. H. L. P. Hydrogen Sulfide Prevents Ethanol-Induced Gastric Damage in Mice: Role of ATP-Sensitive Potassium Channels and Capsaicin-Sensitive Primary Afferent Neurons. *J. Pharmacol. Exp. Ther.* **2009**, *330*, 764–770.
- (59) Medeiros, J. V. R.; Gadelha, G. G.; Lima, S. J.; Garcia, J. A.; Soares, P. M. G.; Santos, A. A.; Brito, G. A. C.; Ribeiro, R. A.; Souza, M. H. L. P. Role of the NO/cGMP/ $K_{ATP}$  pathway in the protective effects of sildenafil against ethanol-induced gastric damage in rats. *Br. J. Pharmacol.* **2008**, *153*, 721–727.
- (60) Damasceno, S. R. B.; Rodrigues, J. C.; Silva, R. O.; Nicolau, L. A. D.; Chaves, L. S.; Freitas, A. L. P.; Souza, M. H. L. P.; Barbosa, A. L. R.; Medeiros, J.-V. R. Role of the NO/KATP pathway in the protective effect of a sulfated-polysaccharide fraction from the algae *Hypnea musciformis* against ethanol-induced gastric damage in mice. *Rev. Bras. Farmacogn.* **2013**, *23*, 320–328.
- (61) Souza, L. K. M.; Nicolau, L. A. D.; Sousa, N. A.; Araújo, T. S. L.; Sousa, F. B. M.; Costa, D. S.; Souza, F. M.; Pacífico, D. M.; Martins, C. S.; Silva, R. O.; et al. Diminazene aceturate, an angiotensin-converting enzyme II activator, prevents gastric mucosal damage in mice: Role of the angiotensin-(1–7)/Mas receptor axis. *Biochem. Pharmacol.* **2016**, *112*, 50–59.
- (62) Matsumoto, T.; Moriguchi, R.; Yamada, H. Role of Polymorphonuclear Leucocytes and Oxygen-derived Free Radicals in the Formation of Gastric Lesions Induced by HCl/ethanol, and a Possible Mechanism of Protection by Anti-ulcer Polysaccharide. *J. Pharm. Pharmacol.* **1993**, *45*, 535–539.
- (63) Trier, J. S.; Szabo, S.; Allan, C. H. Ethanol-induced damage to mucosal capillaries of rat stomach. Ultrastructural features and effects of prostaglandin  $F_{2\beta}$  and cysteamine. *Gastroenterology* **1987**, *92*, 13–22.
- (64) Guslandi, M. Effects of Ethanol on the Gastric Mucosa. *Dig. Dis.* **1987**, *5*, 21–32.
- (65) Santos, P. L.; Brito, R. G.; Quintans, J. S. S.; Araujo, A. A. S.; Menezes, I. R. A.; Brogden, N. K.; Quintans-Junior, L. J. Cyclodextrins as Complexation Agents to Improve the Anti-inflammatory Drugs Profile: a Systematic Review and Meta-Analysis. *Curr. Pharm. Des.* **2017**, *23*, 2096–2107.
- (66) Lima, P. S. S.; Lucchese, A. M.; Araújo-Filho, H. G.; Menezes, P. P.; Araújo, A. A. S.; Quintans-Júnior, L. J.; Quintans, J. S. S. Inclusion

of terpenes in cyclodextrins: Preparation, characterization and pharmacological approaches. *Carbohydr. Polym.* **2016**, *151*, 965–987.

(67) Rakmai, J.; Cheirsilp, B.; Mejuto, J. C.; Torrado-Agrasar, A.; Simal-Gándara, J. Physico-chemical characterization and evaluation of bio-efficacies of black pepper essential oil encapsulated in hydroxypropyl-beta-cyclodextrin. *Food Hydrocolloids* **2017**, *65*, 157–164.

(68) Santos, E. H.; Kamimura, J. A.; Hill, L. E.; Gomes, C. L. Characterization of carvacrol beta-cyclodextrin inclusion complexes as delivery systems for antibacterial and antioxidant applications. *LWT – Food Sci. Technol.* **2015**, *60*, 583–592.

(69) Hess, B.; Kutzner, C.; van der Spoel, D.; Lindahl, E. GROMACS 4: Algorithms for Highly Efficient, Load-Balanced, and Scalable Molecular Simulation. *J. Chem. Theory Comput.* **2008**, *4*, 435–447.

(70) Schuler, L. D.; Daura, X.; van Gunsteren, W. F. An improved GROMOS96 force field for aliphatic hydrocarbons in the condensed phase. *J. Comput. Chem.* **2001**, *22*, 1205–1218.

(71) Kleywegt, G. J.; Jones, T. A. Databases in Protein Crystallography. *Acta Crystallogr., Sect. D: Biol. Crystallogr.* **1998**, *54*, 1119–1131.

(72) Kleywegt, G. J.; Henrick, K.; Dodson, E. J.; van Aalten, D. M. F. Pound-Wise but Penny-Foolish. *Structure* **2003**, *11*, 1051–1059.

(73) Kleywegt, G. J. Crystallographic refinement of ligand complexes. *Acta Crystallogr., Sect. D: Biol. Crystallogr.* **2007**, *63*, 94–100.

(74) Malde, A. K.; Zuo, L.; Breeze, M.; Stroet, M.; Poger, D.; Nair, P. C.; Oostenbrink, C.; Mark, A. E. An Automated Force Field Topology Builder (ATB) and Repository: Version 1.0. *J. Chem. Theory Comput.* **2011**, *7*, 4026–4037.

(75) Essmann, U.; Perera, L.; Berkowitz, M. L.; Darden, T.; Lee, H.; Pedersen, L. G. A smooth particle mesh Ewald method. *J. Chem. Phys.* **1995**, *103*, 8577–8593.

(76) Hess, B.; Bekker, H.; Berendsen, H. J. C.; Fraaije, J. G. E. M. LINCS: A linear constraint solver for molecular simulations. *J. Comput. Chem.* **1997**, *18*, 1463–1472.

(77) Humphrey, W.; Dalke, A.; Schulten, K. VMD: Visual molecular dynamics. *J. Mol. Graphics* **1996**, *14*, 33–38.

(78) Bradley, P. P.; Christensen, R. D.; Rothstein, G. Cellular and extracellular myeloperoxidase in pyogenic inflammation. *Blood* **1982**, *60*, 618–622.

(79) Sedlak, J.; Lindsay, R. H. Estimation of total, protein-bound, and nonprotein sulfhydryl groups in tissue with Ellman's reagent. *Anal. Biochem.* **1968**, *25*, 192–205.

(80) Uchiyama, M.; Mihara, M. Determination of malonaldehyde precursor in tissues by thiobarbituric acid test. *Anal. Biochem.* **1978**, *86*, 271–278.

(81) Prado, W. A.; Schiavon, V. F.; Cunha, F. Q. Dual effect of local application of nitric oxide donors in a model of incision pain in rats. *Eur. J. Pharmacol.* **2002**, *441*, 57–65.